Liquid Jet Response to Detonation Waves in a Linear Detonation Combustor

Charles H. Black*, Timothy R. Winter†, Deborah R. Jackson‡, Mark D. Frederick§, Rohan M. Gejji ¶, Carson D. Slabaugh ‖
Purdue University, West Lafayette, IN, 47906

H. Douglas Perkins **
NASA Glenn Research Center, Cleveland, OH 44135, USA

Christopher A. Fugger ††
Spectral Energies LLC, Beavercreek, OH, 45430

The impact of periodic detonation wave impact on a liquid fuel jet is investigated in a linear detonation combustor. The linear detonation combustor operated with gaseous natural gas and oxygen generates sustained, self-excited detonation waves that propagate along its length at approximately 8 kHz, representing a wave propagation frequency in typical rocket rotating detonation engines. The effect of the detonation wave on the dynamic injection and break-up of a single diesel jet injected into the combustion chamber at varying injection pressures is evaluated with chemiluminescence, fuel planar laser induced fluorescence and Mie scattering measurements at 100 kHz. The detonation wave significantly impacts the liquid jet trajectory with its deflection in both windward and leeward direction as the adverse pressure gradient across it changes between wave passages. The maximum recovery height of the liquid jet is observed to be consistent across all operating conditions, and dependent on the detonation wave strength in the chamber.

I. Introduction

Rotating detonation engines (RDEs) are a means of utilizing the rapid energy release from detonations for more efficient and compact propulsion and power generation, compared to traditional combustion systems [1–4]. RDEs typically operate with an annular combustion chamber with their operation defined by number of detonation waves, their strength, and direction of propagation. These parameters vary significantly with device size and geometry, combination of reactants used, and operating parameters [5–10]. The study of different aspects of RDE operability and performance have predominantly focused on the use of gaseous propellants over the last two decades. Several propulsion applications rely on liquid phase injection of one or both propellants due to their high-energy and storability [11–18]. Characterization of liquid fuel injection and its impact of RDE operability and performance is critical for its development as a viable technology for liquid rocket engines.

The multiphase nature of liquid fueled RDEs introduces additional complexity to the RDE flowfield as the liquid fuels must undergo breakup, atomization, evaporation, and mixing before reaction. Fuel droplets introduce heterogeneity that fundamentally alters the detonation-wave characteristics and morphology in contrast to their gas-phase counterpart. The timescales for droplet breakup, evaporation, and mixing impact net reaction rates, detonation peak pressure, and velocity. The significantly lower volume fraction occupied by liquid fuels compared to the gaseous oxidizer surrounding it can result in wide spatiotemporal variations in fuel-oxidizer ratio, resulting in incomplete combustion that further decreases the energy available to the detonation wave. These rate-controlling processes are thus of fundamental importance to predicting the vapor production and net reaction rates in multiphase detonations. To accurately understand the impact of

*Graduate Research Assistant, School of Aeronautics and Astronautics, West Lafayette, IN, AIAA Student Member.
†Graduate Research Assistant, School of Aeronautics and Astronautics, West Lafayette, IN, AIAA Student Member.
‡Graduate Research Assistant, School of Aeronautics and Astronautics, West Lafayette, IN, AIAA Student Member.
§Graduate Research Assistant, School of Aeronautics and Astronautics, West Lafayette, IN, AIAA Student Member.
¶Research Engineer, School of Aeronautics and Astronautics, West Lafayette, IN, AIAA Senior Member.
‖Associate Professor, School of Aeronautics and Astronautics, West Lafayette, IN, AIAA Associate Fellow.
**Aerospace Engineer, NASA Glenn Research Center, Cleveland, OH 44135, USA, AIAA Member
††Sr. Research Engineer, Spectral Energies, LLC, 4065 Executive Dr. Beavercreek, OH 45430, USA AIAA Senior Member

these processes on macroscale properties of the RDE - wave number and direction, wave-speed, operability envelope and performance - laser and imaging based diagnostics in an optically accessible experiment with a relevant canonical liquid injector can play an important role in the development of liquid-fueled RDEs.

The specific objectives of the proposed study are to investigate the injection, mixing, break-up of the liquid fuel droplets in an optically accessible detonation wave based combustor. In the current experiment, a single liquid jet is injected into a linear detonation combustor operated with natural gas and oxygen. The linear detonation combustor generates sustained, self-excited detonation waves that propagate along its length at approximately 8 kHz, closely representing a wave propagation frequency in rocket RDEs. Laser and imaging based diagnostics are used to study the influence of the detonation wave on the liquid fuel injector at a range of injection pressure ratios. Detonation wave characteristics are characterized using an array of high frequency pressure measurements, OH*-chemiluminescence, liquid fuel PLIF, and Mie scattering measurements.

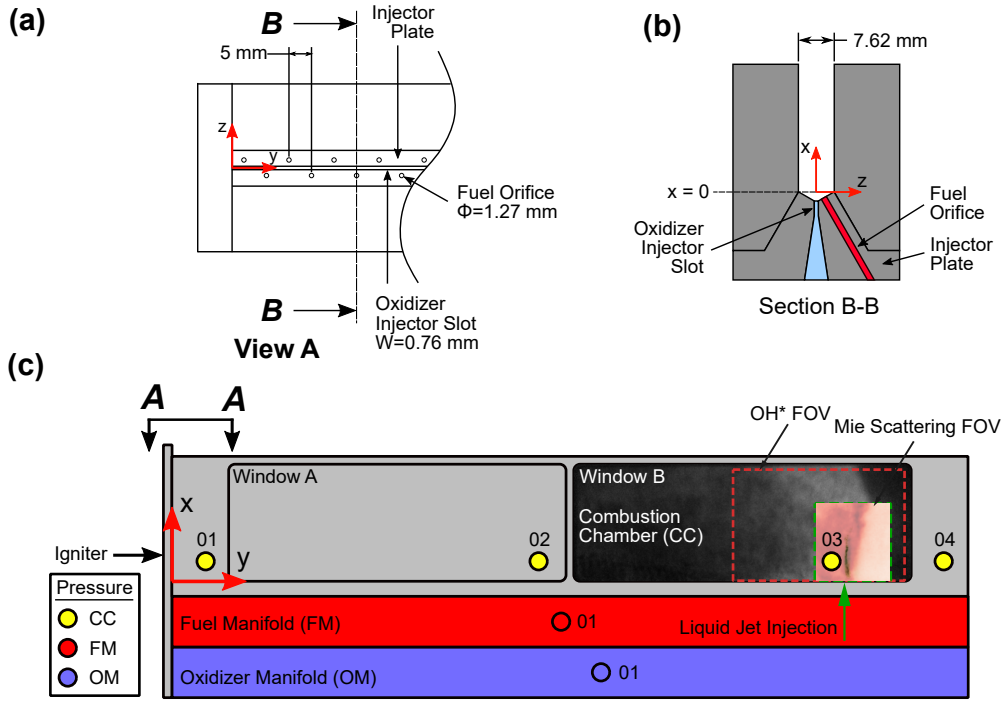

Fig. 1 Schematic representation of the linear detonation combustor.

II. Experimental Description

A. Linear Detonation Channel

A single liquid kerosene jet was introduced in the linear detonation combustor to characterize the effect of periodic detonation wave on its break-up. Figure 1 depicts the self-excited linear detonation combustor used in this study [9, 10, 19]. Gaseous oxygen was injected axially (+X-direction) through a 0.76 mm wide slot spanning the transverse (Y-direction) length of the combustor. Natural gas (NG) was introduced at an angle of 30° relative to the +X-direction through 1.27 mm orifices distributed on alternating sides along the length of the oxidizer injector. Influence of combustion dynamics on the reactant feed supply was isolated using sonic orifices installed at each reactant manifold inlet. Combustion products were exhausted through an axial (X = 90 mm) and transverse (Y = 610 mm) combustion chamber exit boundary. Reactant mass flow rates were metered with critical flow venturi nozzles which provided a measurement uncertainty of 1.5%. Fused quartz windows installed on either side of the Window B region provide optical access to the chamber. In the current study, single-point liquid jet was injected from a plain orifice atomizer, 0.381 mm in diameter, co-axially with the oxidizer flow. The nearest NG injection sites on either side of the liquid injector were plugged to minimize influence of NG jets on the liquid fuel column. The liquid fuel manifold was designed

to minimize impact of its location in the oxidizer manifold on the oxidizer flow-path into the combustion chamber. Figure 2 shows a schematic representation of the injector and its installation in the oxidizer manifold. The injection location was located at approximately Y = 500 mm, to ensure the detonation wave was fully developed by the time it reached the liquid jet. Diesel was used as the liquid fuel for the results presented in the current work.

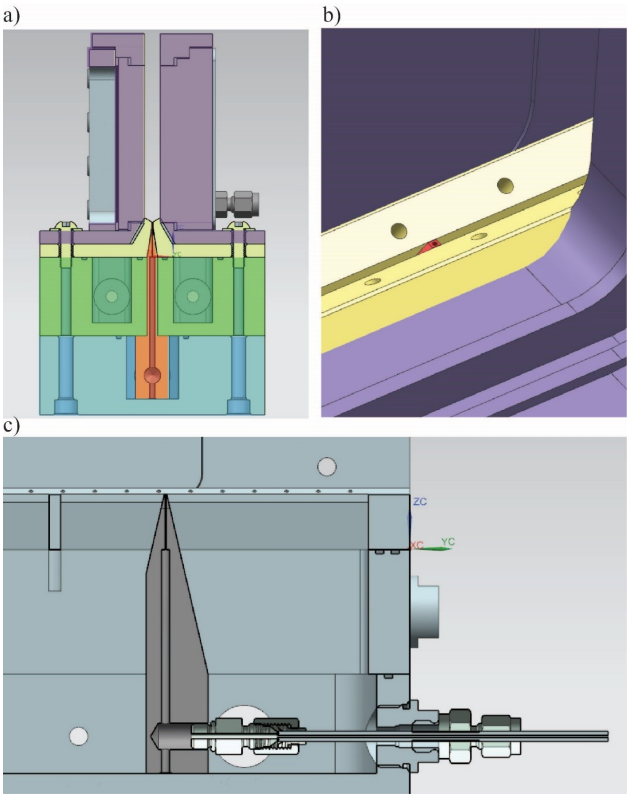

Fig. 2 Schematic representation of the single-point liquid fuel injector.

B. Diagnostics Configuration

High-frequency (HF) pressure measurements were acquired at the locations shown in Fig. 1(c) to characterize chamber dynamics throughout each test. Piezoelectric pressure transducers (PCB 113B26), sampled at 2 MHz, were installed flush with the chamber walls to measure dynamic pressure in the experiment. Static pressures in the propellant manifolds and combustion chamber were measured at 2 MHz using piezoresistive pressure transducers (Kulite WCT312M). Gaseous flow rate monitoring was achieved using pressure transducers (GE-UNIK 50E6) and type-K thermocouples (Omega GKMQIN-062G) immediately upstream of critical flow venturi nozzles (CFVN) that conform to ISO 9300 specifications. The pressure drop across each CFVN was monitored to ensure a choked condition throughout the test duration despite the highly dynamic processes occurring downstream. Liquid fuel flow rate was similarly monitored with pressure and temperature measurements upstream of a cavitating venturi nozzle.

Chemiluminescence images of hydroxyl radicals (OH^*-CL) were obtained at 100 kHz in the XY plane field of view (FoV) to resolve the path-integrated evolution of heat-release within the chamber. A spectral filter centered at 320 nm with a ±20 nm bandwidth was used to isolate background luminosity from OH^*-CL signal. The signal was collected with a 100 mm focal-length, f/2.8 objective lens (Cerco Sodern Type-2178) and recorded with a Phantom v411 CMOS camera. Mie scattering and fuel-PLIF measurements were conducted using a Nd:YAG-based master oscillator power amplifier Pulse-Burst Laser (PBL) system (Spectral Energies QuasiModo) and high-speed CMOS cameras (two Phantom v2512s). Both the frequency doubled (532 nm) and tripled (355 nm) outputs from the PBL were delivered at a repetition frequency of 100 kHz in a 10 ms pulse train, yielding approximately 1000 images. The beams were expanded and collimated using cylindrical lenses in a telescope arrangement and then focused using two additional cylindrical lenses, for both laser beams. The laser sheets were focused just beyond the measurement plane to achieve

a near-constant laser sheet thickness of 600 μm while avoiding an increase in signal drop-out near the beam waist. The PLIF scattering signal was imaged using a 200 mm $f/4.0$ lens (Nikon AF Micro NIKKOR) with a 3-nm FWHM bandpass filter, amplified by a Lambert HiCATT25 intensifier, and recorded with a second Phantom v2512 high-speed CMOS camera. The PLIF signal was spectrally isolated from background chemiluminescence with a 375 nm long pass filter and a 400±25 nm band-pass filter.

III. Results

Pressure time history from a representative test is shown in Fig. 3(a-b). A short transient follows ignition at time t = 0 s after which limit-cycle, periodic detonation wave generation. OH^*-CL measurements are obtained over the test duration (~250 ms) while PLIF images were recorded after steady dynamics are achieved in the experiment. Figure 3(c) provides a time series of binned OH^*-CL signal collected near the injection surface to illustrates periodic detonation wave generation. Each dark line represents a detonation wave propagating in the $+Y$-direction while its slope represents detonation wave speed. A summary of operating conditions for cases examined in this study are provided in Table 1. These cases represent a low, medium, and high liquid injection stiffness and velocity while the natural gas and O_2 operating parameters are held fixed. This enables study of discriminating liquid jet dynamics when subjected to a relatively constant forcing frequency (~8 kHz) and amplitude.

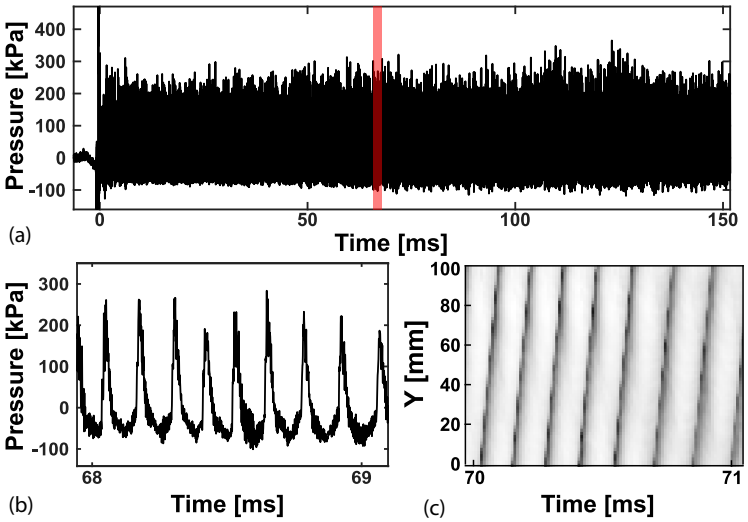

Fig. 3 Pressure amplitude measured for a representative test at CC-03 along with a magnified view. OH^*-CL signal collected near the injection surface along the XY FoV width is shown at bottom right.

Table 1 Summary of operating conditions

Case	Chamber Mass Flux $[kg/s-m^2]$	Global ϕ [-]	$\dot{m}_{liq}$ $[g/s]$	$P_{Manifold_{Liq}}$ [kPa]
1	134	0.88	1.19	224.1
2	134	0.88	1.70	344.8
3	134	0.86	2.10	652.4

A time series of overlaid chemiluminesence (red) and fuel-PLIF (blue) images, highlighting the liquid jet trajectory after the passage of a detonation wave and its subsequent consumption by the next wave for Case 1 are shown in Figure 4. The time separation between consecutive frames is 10 μs. The sequence of images start midway between two consecutive detonation wave passages with the wave impact with the jet occurring at ~40 μs. To characterize the liquid

jet displacement and recovery, the centerline of the jet is identified based on an intensity based reduction of the overall fuel-PLIF intensity. In the region where the jet is present, the weighted average of the signal intensity at each location in the x direction is evaluated. The peak value of this row-wise weighted average is demarcated as the jet centerline. Regions along the centerline with low PLIF intensity along the centerline are disregarded from the jet length, and pockets downstream of such regions represent pockets of fuel, liquid or gas that have been sheared from the liquid jet column.

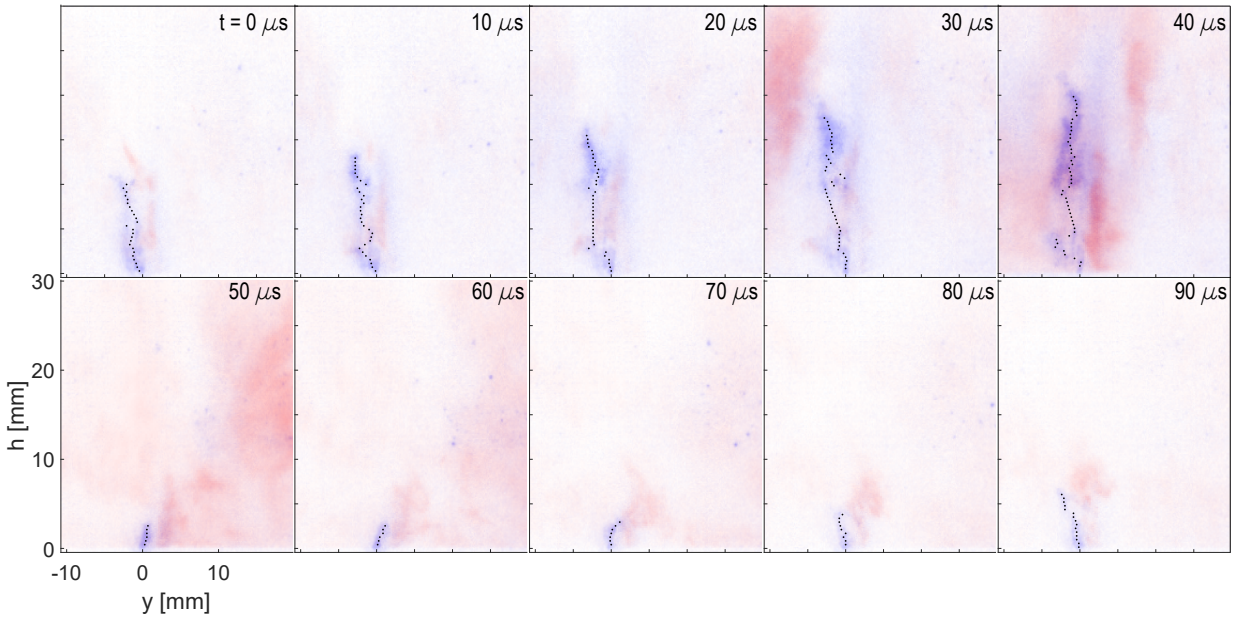

Fig. 4 Overlaid chemiluminescence (red) and kerosene PLIF (blue) images from Case 1. The centerline of the liquid fuel jet is tracked and shown with the black dots.

The liquid jet is significantly impacted by the detonation wave, with displacement, break-up and consumption in the direction of the wave (left–right) immediately following its passage. As the jet recovers, its trajectory is in the windward direction corresponding to adverse pressure gradient downstream of the detonation wave. At the lowest fuel supply pressure in this study (225 kPa), the liquid fuel is almost entirely consumed by the detonation wave, however trace amounts of fuel remain at the injection site and no evidence of combustion product back-flow into the injector is observed. The jet column height stays constant for a period up 40 μs, before a linear recovery to its full height before arrival of the next detonation wave.

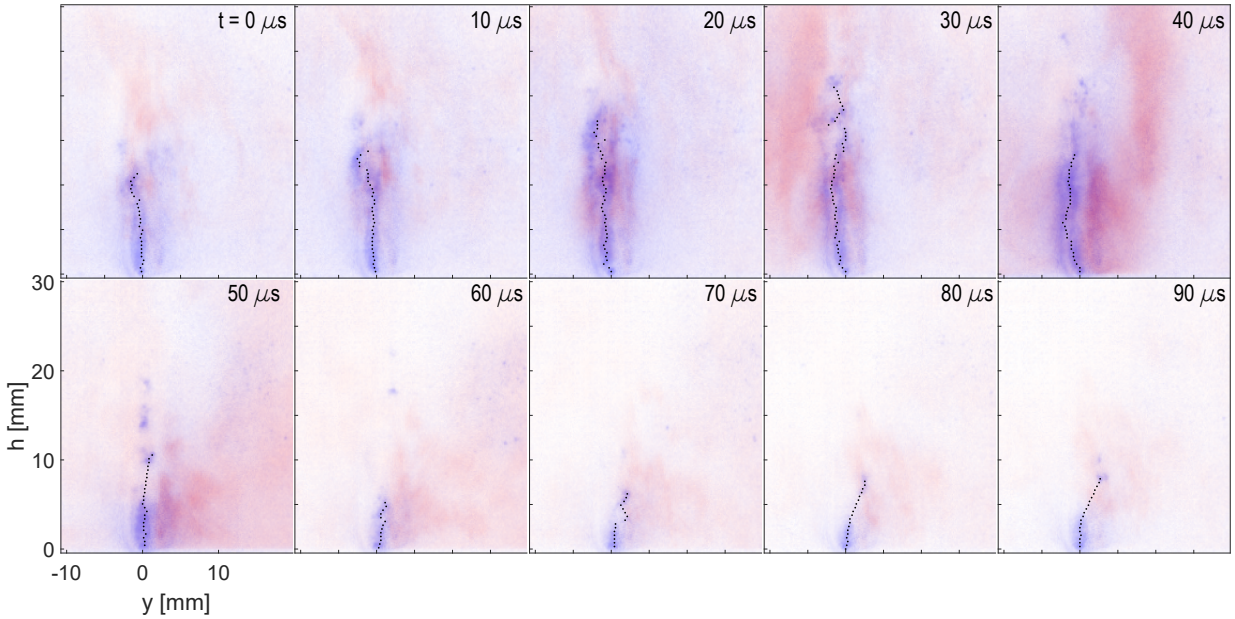

Fig. 5 Overlaid chemiluminescence (red) and kerosene PLIF (blue) images from Case 2. The centerline of the liquid fuel jet is tracked and shown with the black dots.

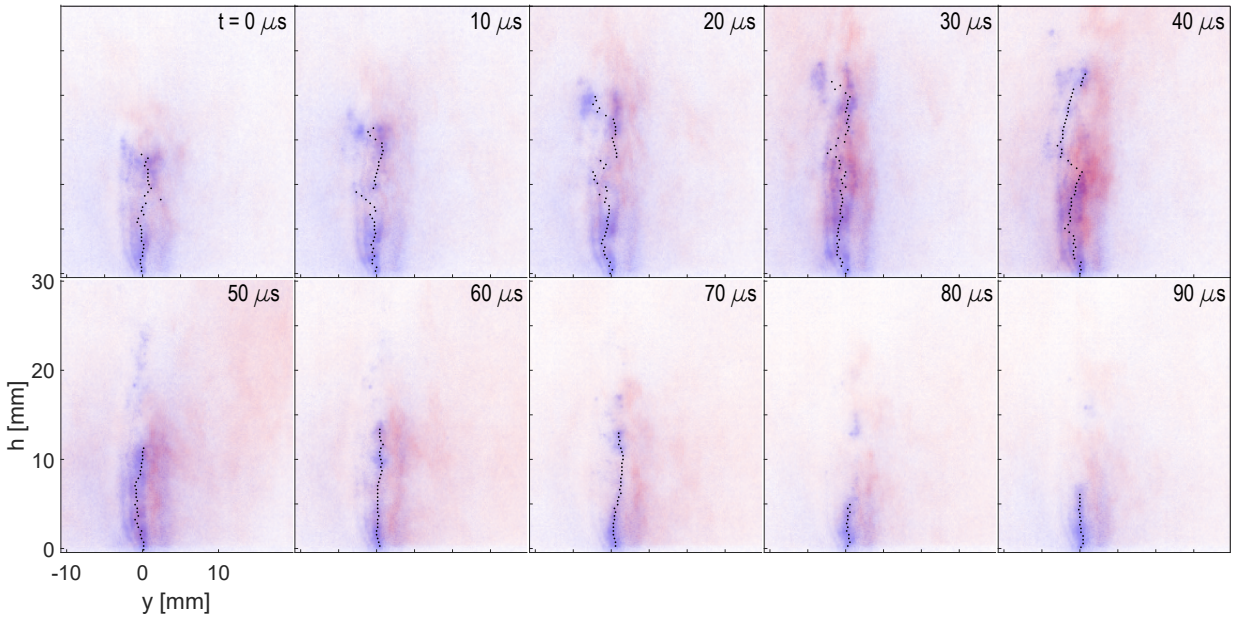

Fig. 6 Overlaid chemiluminescence (red) and kerosene PLIF (blue) images from Case 3. The centerline of the liquid fuel jet is tracked and shown with the black dots.

A time series of overlaid chemiluminesence (red) and fuel-PLIF (blue) images for Case 2 are shown in Figure 4. With an ~35% increase in fuel supply pressure, the liquid jet recovery occurs at much faster rate in comparison with Case 1. As more diesel is injected between wave passages, it is qualitatively evident that a larger fraction is present in the channel throughout all axial locations compared to Figure 4. The liquid jet column deflects leeward (+Y) as the fuel travels at some velocity induced by the passing detonation wave. As the jet recovers, due to relatively low local pressure and velocity in the channel, its trajectory is primarily vertical with minimal displacement in the windward

direction before the arrival of the next detonation wave. The cycle averaged liquid column across all cases was found to be inclined in the -Y direction indicating that the mean axial momentum is likely forcing the column in that direction. This is consistently observed at all operating conditions, however is more pronounced at lower liquid supply pressures. For all test cases presented in the current work, the detonation wave propagation was consistently in the +Y direction at all times with a near uniform wave speed of 1480 m/s. The maximum jet column height for Case 2 is similar to that observed in Case 1, despite a higher column present immediately after wave passage (at 60 μs) than Case 1.

In Figure 6, the liquid column is more resilient to detonation wave impact and insignificant reduction in its height is observed for as much as 30 μs after wave passage. The intact column height reduces at 80 and 90 μs, which may correspond to the consumption of the diesel after vaporization and mixing with combustion products and oxidizer from the previous wave passage. The relative increase in chemiluminesence intensity at these time instants (60-80 μs) compared to Case 1 and 2 is indicative of this slow deflagrative burning of the remaining diesel in the channel. The jet recovers immediately afterwards, with a noticeable increase in height by the T+90 μs frame. Additionally, the high momentum of the liquid jet in Case 3 results in a vertical jet trajectory with no inclination, either in the windward or leeward directions during its recovery to full column height. The maximum jet height for Case 3 is similar in magnitude to Cases 1 and 2 highlighting its insensitivity to liquid fuel supply pressure.

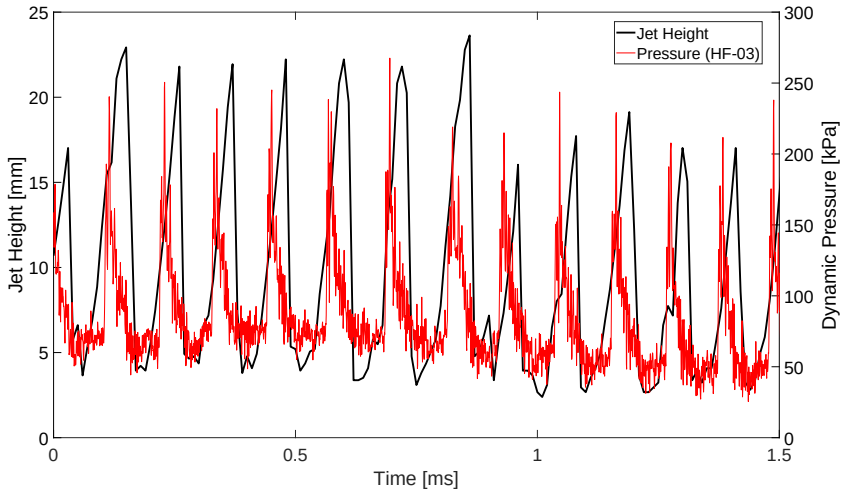

Fig. 7 Liquid column height and dynamic pressure as measured in the combustion chamber for Case 1

The dynamic pressure in the detonation channel was measured using a high frequency pressure transducer (PCB 113B26) at 2 MHz, located approximately 36 mm upstream of the location of liquid fuel injection. at an average detonation wave speed of ~1480 m/s [10], this corresponds to a time delay of 24 μs for the wave to arrive at the location of fuel injection. The delay is consistent with the advance in time arrival of the pressure wavefront with respect to the decrease in liquid column height from its interaction with the wave. In Figure 7, it can be seen that the liquid jet height steadily increases up to the point of detonation wave arrival followed by its decrease to a minimum jet height within 10 μs of wave arrival. Following jet interaction with the wave, and the concomitant reversal in pressure drop across the injector upon its passage, jet recovery is initiated. For Case 1, the liquid fuel appears to spend approximately 40-50 % of the time dwelling at a minimum height, before spending approximately the same amount of time in recovery. The jet recovery is observed to be fairly linear during this period.

Table 2 Summary of key metrics of the liquid jet characteristics

Case	$P_{Manifold_{Liq}}$ [kPa]	$\bar{h}_{max}$ [mm]	$\bar{h}$ [mm]	$\bar{h}_{min}$ [mm]	$\tau_{filling}$ [μs]	τ_{dwell} [μs]
1	224.1	19.89	9.19	2.86	85	48
2	344.8	19.76	10.94	5.35	79	46
3	652.4	19.74	12.00	6.14	77	41

The instantaneous height of the liquid column, as well as the minimum post-wave height, increases with an increase liquid mass flow rate and injection pressure. A reverse trend is observed for the time-averaged mean column height as a function of supply pressure. While a clear trend in the time averaged minimum, mean, and maximum liquid column heights is apparent across the three injection pressures in the current study, the sensitivity of this parameter to jet momentum, break-up, vaporization, and consumption in the combustion chamber need further evaluation.

The liquid column, while not completely consumed, does dwell at a minimum height for a period of time after the wave has passed and before the injector has pushed enough fuel into the column to increase its height. This dwell time was seen to decrease at increased liquid injection pressures, indicating that the injector itself recovers more quickly at a higher mass flow. The fill time of the jet is defined as the time required for the jet to reach its maximum height from its minimum location between detonation wave passages. A summary of time averaged jet column heights and respective dwell and fill times are summarized in Table 2. The liquid jet cycle can be broken up into three phases: fill, dwell, and consumption. The refill time was observed to decrease with an increase in liquid injection pressure. It appears that, as injection pressure increases, the consumption phase lasts longer, as the dwell and filling time decrease. This is evident in Figure 6, as the liquid jet takes a considerable amount of time to be consumed before its short dwell.

IV. Conclusion

The impact of periodic detonation wave impact on a liquid fuel jet was investigated in a linear detonation combustor. The linear detonation combustor operated with gaseous natural gas and oxygen generates sustained, self-excited detonation waves that propagate along its length at approximately 8 kHz, representing a wave propagation frequency in typical rocket rotating detonation engines. The effect of the detonation wave on the dynamic injection and break-up of a single diesel jet injected into the combustion chamber at varying injection pressures is evaluated with chemiluminescence, fuel planar laser induced fluorescence and Mie scattering measurements at 100 kHz.

The influence of injection pressure on the liquid fuel recovery and jet height was investigated using fuel-PLIF images. The maximum jet height was observed to be relatively insensitive to supply pressure, even as trends in jet trajectory and recovery time were evident across investigated test cases. The insensitivity to jet height might indicate increase in fuel break-up, vaporization, and potentially consumption in the presence of warm oxidizer and combustion products from the previous wave passage balancing the additional momentum carried by the jet with injector pressure drops. The detonation wave significantly impacted the liquid jet trajectory with its deflection in both windward and leeward direction as the adverse pressure gradient across it changes between wave passages.

Acknowledgments

This work was funded by NASA STTR contract 80NSSC21C0031. The high-speed cameras used in this work were purchased with DURIP grants FA9550-20-1-0226 and FA9550-16-1-0534 (Program Manager: Dr. Chiping Li).

References

[1] Lu, F. K., and Braun, E. M., "Rotating Detonation Wave Propulsion: Experimental Challenges, Modeling, and Engine Concepts," *Journal of Propulsion and Power*, Vol. 30, No. 5, 2014, pp. 1125–1142. https://doi.org/10.2514/1.b34802.

[2] Wolanski, P., "Detonative Propulsion," *Proceedings of the Combustion Institute*, Vol. 34, No. 1, 2013, pp. 125–158. https://doi.org/10.1016/j.proci.2012.10.005.

[3] Bykovskii, F. A., Zhdan, S. A., and Vedernikov, E. F., "Continuous Spin Detonations," *Journal of Propulsion and Power*, Vol. 22, No. 6, 2006, pp. 1204–1216. https://doi.org/10.2514/1.17656.

[4] Kailasanath, K., and Schwer, D. A., "High-Fidelity Simulations of Pressure-Gain Combustion Devices Based on Detonations," *Journal of Propulsion and Power*, Vol. 33, No. 1, 2017, pp. 153–162. https://doi.org/10.2514/1.B36169.

[5] Bennewitz, J. W., Bigler, B. R., Pilgram, J. J., and Hargus, Jr., W. A., "Modal Transitions in Rotating Detonation Rocket Engines," *International Journal of Energetic Materials and Chemical Propulsion*, Vol. 18, No. 2, 2019, pp. 91–109. https://doi.org/10.1615/intjenergeticmaterialschemprop.2019027880.

[6] Walters, I. V., Journell, C. L., Lemcherfi, A., Gejji, R. M., Heister, S. D., and Slabaugh, C. D., "Operability of a Natural Gas–Air Rotating Detonation Engine," *Journal of Propulsion and Power*, Vol. 36, No. 3, 2020, pp. 453–464. https://doi.org/10.2514/1.B37735.

[7] Plaehn, E. W., Gejji, R. M., Walters, I. V., and Slabaugh, C. D., "Equivalent Supply Pressure for Pressure Gain Estimation in Rotating Detonation Engines," *Journal of Propulsion and Power*, Vol. 0, No. 0, 0, pp. 1–5. https://doi.org/10.2514/1.B39009, URL https://doi.org/10.2514/1.B39009.

[8] Plaehn, E. W., Walters, I. V., Gejji, R. M., and Slabaugh, C. D., "Bifurcation in Rotating Detonation Engine Operation with Continuously Variable Fuel Injection Location," *Journal of Propulsion and Power*, Vol. 0, No. 0, 2022, pp. 1–15. https://doi.org/10.2514/1.B38801, URL https://doi.org/10.2514/1.B38801.

[9] Ayers, Z. M., Lemcherfi, A., Plaehn, E. W., Gejji, R. M., Perkins, H. D., Roy, S., Slabaugh, C. D., Meyer, T. R., and Fugger, C. A., "Simultaneous 100-kHz acetone planar laser-induced fluorescence and OH* chemiluminescence in a linear non-premixed detonation channel," *Combustion and Flame*, Vol. 244, 2022, p. 112209. https://doi.org/https://doi.org/10.1016/j.combustflame.2022.112209, URL https://www.sciencedirect.com/science/article/pii/S0010218022002243.

[10] Lemcherfi, A., Gejji, R. M., Ayers, Z. M., Plaehn, E. W., Perkins, H. D., Roy, S., Meyer, T. R., Fugger, C. A., and Slabaugh, C. D., "Effect of injection dynamics on detonation wave propagation in a linear detonation combustor," *Proceedings of the Combustion Institute*, 2022. https://doi.org/https://doi.org/10.1016/j.proci.2022.08.004, URL https://www.sciencedirect.com/science/article/pii/S154074892200270X.

[11] Anderson, W. S., and Heister, S. D., "Response of a Liquid Jet in a Multiple-Detonation Driven Crossflow," *Journal of Propulsion and Power*, Vol. 35, No. 2, 2019, pp. 303–312. https://doi.org/10.2514/1.B37127.

[12] Anderson, W. S., Heister, S. D., Kan, B., and Hartsfield, C., "Experimental Study of a Hypergolically Ignited Liquid Bipropellant Rotating Detonation Rocket Engine," *Journal of Propulsion and Power*, Vol. 36, No. 6, 2020, pp. 851–861. https://doi.org/10.2514/1.B37666.

[13] Li, J.-M., Chang, P.-H., Li, L., Yang, Y., Teo, C. J., and Khoo, B. C., *Investigation of Injection Strategy for Liquid-Fuel Rotating Detonation Engine*, 2018. https://doi.org/10.2514/6.2018-0403.

[14] Lim, D., "Experimental Studies of Liquid Injector Response and Wall Heat Flux in a Rotating Detonation Rocket Engine," 2019. https://doi.org/10.25394/PGS.11113250.v1.

[15] Kindracki, J., "Experimental research on rotating detonation in liquid fuel–gaseous air mixtures," *Aerospace Science and Technology*, Vol. 43, 2015, pp. 445–453. https://doi.org/10.1016/j.ast.2015.04.006.

[16] Harroun, A., and Heister, S. D., *Liquid Fuel Survey for Rotating Detonation Rocket Engines*, 2022. https://doi.org/10.2514/6.2022-0088, URL https://arc.aiaa.org/doi/abs/10.2514/6.2022-0088.

[17] Humble, J., and Heister, S. D., *Heterogeneous Detonation Physics as Applied to High Pressure Rotating Detonation Engines*, 2021. https://doi.org/10.2514/6.2021-1027.

[18] Hoeper, M. W., Webb, A. M., Athmanathan, V., Wang, R. B., Douglas Perkins, H., Roy, S., Meyer, T. R., and Fugger, C. A., "Liquid fuel refill dynamics in a rotating detonation combustor using megahertz planar laser-induced fluorescence," *Proceedings of the Combustion Institute*, 2022. https://doi.org/https://doi.org/10.1016/j.proci.2022.07.230, URL https://www.sciencedirect.com/science/article/pii/S154074892200267X.

[19] Schwinn, K., Gejji, R., Kan, B., Sardeshmukh, S., Heister, S., and Slabaugh, C. D., "Self-sustained, high-frequency detonation wave generation in a semi-bounded channel," *Combustion and Flame*, Vol. 193, 2018, pp. 384–396. https://doi.org/10.1016/j.combustflame.2018.03.022.